

A DESIGN OF TWISTED DOUBLE CHANNEL SCISSORS FOR OPTICAL FILTER

H. M. Hairi^{1,2}, T. Saktioto^{2,3}, Dedi Irawan², J. Ali²

¹Department of Applied Science, Universiti Teknologi MARA Pulau Pinang, Permatang Pauh, 13500, Pulau Pinang, Malaysia

²Advanced Photonics and Science Institutes, Faculty of Science, Universiti Teknologi Malaysia, 81310 Skudai, Johor Bahru, Malaysia.

³University of Riau, Pekanbaru, 28293, Riau, Indonesia.

ABSTRACT

Microring resonators have emerged in the past few years in integrated optics and have been used extensively in many fields due to its advantages. The response from coupled ring resonators can be custom designed by the use of different coupling configurations [1]. In certain cases, ring resonators can be used as wavelength filter when the wavelength fits a whole multiple times in the circumference of the ring [5,6]. In this paper, we compare and contrast the effect of light propagation/ power distribution characteristics associated with ring configurations. We have limited our study to side-coupled integrated space sequence of resonators or as known as SCISSORS using OptiFDTD Photonics Simulation Software V8.0.

Keywords: *Microring resonator; Side-coupled integrated space sequence of resonators; power distribution.*

I. Introduction

The Finite Difference Time Domain (FDTD) approach is based on a direct numerical solution of time dependent Maxwell's curl equations. In Figure 1, the photonic device is laid out in the X-Z plane. The propagation is along Z- plane. The Y-direction is assumed to be infinite. This assumption removes all the $\partial/\partial y$ derivatives from Maxwell's equations and splits them into

two either Transverse Electric (TE) or Transverser Magnetic (TM) independent sets of equation.

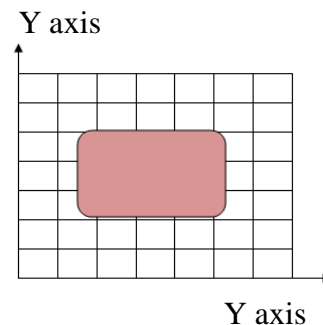


Figure 1: Numerical representation of the 2D computational device

Consider the 2D TE case where H_x , E_y , H_z – nonzero components, propagation along Z, transverse field variations along X using lossless media, Maxwell's equations take the following form:

$$\left. \begin{aligned} \frac{\partial E_y}{\partial t} &= \frac{1}{\varepsilon} \left(\frac{\partial H_x}{\partial z} - \frac{\partial H_z}{\partial x} \right), \\ \frac{\partial H_x}{\partial t} &= \frac{1}{\mu_0} \frac{\partial E_y}{\partial z}, \\ \frac{\partial H_z}{\partial t} &= \frac{1}{\mu_0} \frac{\partial E_y}{\partial x} \end{aligned} \right\} (1)$$

where $\varepsilon = \varepsilon_0 \varepsilon_r$ is the dielectric permittivity and μ_0 is the magnetic permeability of the vacuum. The refractive index is $n \approx \sqrt{\varepsilon_r}$.

Each field is represented by a 2D array – $E_y(i, k)$, $H_x(i, k)$ and $H_z(i, k)$ – corresponding to the 2D mesh grid given in Figure 1. The indices i and k account for the number of space steps in the X and Z direction, respectively. In the case of TE, the location of the fields in the mesh is shown in Figure 2

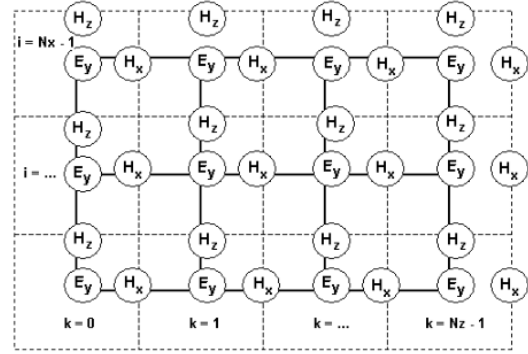


Figure 2: TE fields in computational domain

The TE fields stencil can be explained as follows. The E_y field locations coincide with the mesh nodes given in Figure 1. In Figure 2, the solid lines represent the mesh given in Figure 1. The E_y field is considered to be the center of the FDTD space cell. The dashed lines form the FDTD cells. The H_x field is associated with integer i and $(k + 0.5)$ indices. The H_z field is associated with $(i + 0.5)$ and integer k indices. The numerical analog in Equation (1) can be derived from the following relation:

$$\frac{\partial E_y}{\partial t} = \frac{1}{\varepsilon} \left(\frac{\partial H_x}{\partial z} - \frac{\partial H_z}{\partial x} \right) (2)$$

By using numerical discretization solution, it results as follows:

$$\frac{E_y^n(i, k) - E_y^{n-1}(i, k)}{\Delta t} = + \frac{1}{\varepsilon} \frac{H_x^{n-1/2}(i, k+1/2) - H_x^{n-1/2}(i, k-1/2)}{\Delta z} - \frac{1}{\varepsilon} \frac{H_z^{n-1/2}(i+1/2, k) - H_z^{n-1/2}(i-1/2, k)}{\Delta x}$$

The total set of numerical Equation (1) takes the form

$$\left. \begin{aligned} E_y^n(i, k) &= E_y^{n-1}(i, k) + \frac{\Delta t}{\varepsilon \Delta z} \left[H_x^{n-1/2}(i, k+1/2) - H_x^{n-1/2}(i, k-1/2) \right] \\ &- \frac{\Delta t}{\varepsilon \Delta x} \left[H_z^{n-1/2}(i+1/2, k) - H_z^{n-1/2}(i-1/2, k) \right] \\ H_x^{n+1/2}(i, k+1/2) &= H_x^{n-1/2}(i, k+1/2) + \frac{\Delta t}{\mu_0 \Delta z} \left[E_y^n(i, k+1) - E_y^n(i, k) \right] \\ H_z^{n+1/2}(i+1/2, k) &= H_z^{n-1/2}(i+1/2, k) - \frac{\Delta t}{\mu_0 \Delta x} \left[E_y^n(i+1, k) - E_y^n(i, k) \right] \end{aligned} \right\} (3)$$

The superscripts n labels the time steps while the indices i and k label the space steps and Δx and Δz along the x and z directions, respectively. This is the so called Yee's numerical scheme applied to the 2D TE case [2, 3]. It uses central difference approximations for the numerical derivatives in space and time, both having second order accuracy. The sampling in space is on a sub-wavelength scale. Typically, 10 to 20 steps per wavelength are required. The sampling in

time is selected to ensure numerical stability of the algorithm. The time step, Δt is determined by the Courant limit [3].

$$\Delta t \leq 1 / \left(c \sqrt{1/(\Delta x)^2 + 1/(\Delta z)^2} \right) (4)$$

According to R. Courant *et. al*, time step must be less than a certain time in many explicit time-marching computer simulations, otherwise the simulation will produce incorrect results.

The fundamental constraint of FDTD method is the step size for both for the time and space. Space and time steps relate to the accuracy, numerical dispersion, and the stability of the FDTD method. In general, to keep the results as accurate as possible, with a low numerical dispersive, the mesh size often quoted is "10 cells per wavelength" meaning that the side of each cell should be $1/10\lambda$ or less at the highest frequency (shortest wavelength)

For suggested mesh size:

$$\text{minimum}(\Delta x, \Delta y, \Delta z) \leq \frac{\lambda_{\min}}{10n_{\max}} (5)$$

where n_{\max} is the maximum refractive index value in the computational domain.

Once the cell size is determined, the maximum size for the time step Δt immediately follows the Courant-Friedrichs-Levy (CFL) condition [3].

The field propagated by the FDTD algorithm is the time domain fields. At each location of the computational domain is given by

$$E_y(x, z) = BG(x, z)\sin(\omega t + \varphi_i) \quad (6)$$

where B is the amplitude of the field at that particular location, G is the wave profile, and φ_i is the corresponding phase. In order to get the full amplitude/phase wave information, we need the stationary complex fields that correspond to the waveform. The complex fields are the source of all useful information, such as output and reflected powers, overlap integrals with modal fields, etc. Those complex fields are calculated by a run time Fourier transform performed in the last time period of the simulation.

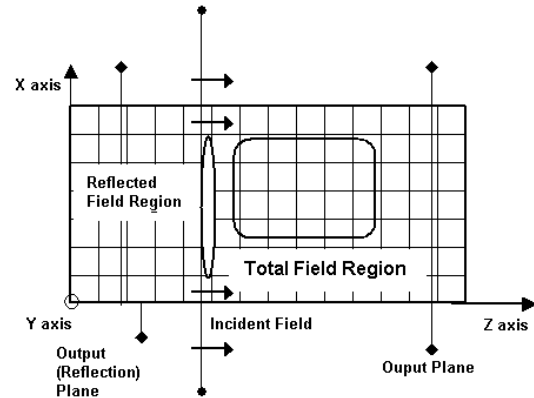


Figure 3: Output Plane [1]

II. DESIGN OF TWISTED DOUBLE CHANNEL SCISSORS

Waveguide structures have been fabricated using several material including InGaAsp, Ta₂O₅/ SiO₂, Si₃N₄, and SiON. It is important to use high refractive index contrast material to reduce bending losses. In this model simulation both microring and waveguide were fabricated from materials that have same characteristics as SiO₂.

In this model, we start the model SiO₂ by setting up the wafer dimensions to 60 μm in length and 20 μm in width. The 2D wafer's refractive index set to air's refractive index which is 1.00. The waveguide being used to model this simulation is set to isotropic constant

refractive index which is its real value of 1.54 and no imaginary part. The device configuration is composed by four ports (2 input ports and 2 output ports) coupled with 5 double ring waveguide and 2 plane waveguide as shown in Figure 4. The details of the configuration are as follows, the length of the both linear waveguide have been set to $60.0 \mu\text{m}$.

Besides the width of fiber is $1.0 \mu\text{m}$. Then, the waveguide is coupled to double ring waveguide with radius of $3.25 \mu\text{m}$, both minor and major radius. The centers of the horizontal position for the upper and lower rings are located at approximately at 8 until $50 \mu\text{m}$ by difference of $22 \mu\text{m}$ between each other. While the vertical position of the upper ring is approximately $4.1 \mu\text{m}$ and

the vertical position are about $-4.1 \mu\text{m}$. The orientation angle of each ring waveguide is 0° .

We have used the default setting for the configuration of channel thickness tapering. The width of the ring is set to $1.0 \mu\text{m}$ and depth of the as the same profile as plane waveguide. The vertical input plane is interfaced to the device as a power source. A continuous wave with wavelength of $1.55 \mu\text{m}$ has been used as the initial properties of the input plane for the Gaussian input field transverse. The plane geometry is set and wave configuration is $0.4 \mu\text{m}$ for its Z position being transverse in positive direction with 0° initial phase. The input power we is 1.0 V/m .

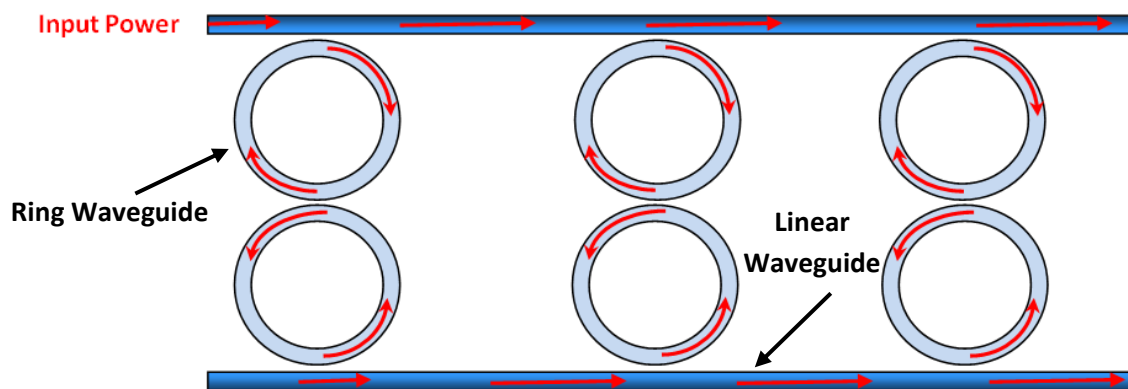


Figure 4: Schematic diagram of twisted doubled channel SCISSORs.

III. RESULTS AND DISCUSSION

Figure 5 shows the model configuration for twisted double channel SCISSORs.

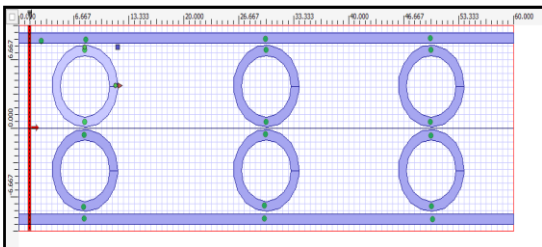


Figure 5: Layout design for the integrated micro ring resonator.

Figure 6 shows the changes of refractive index in the medium when power propagated throughout the bus waveguide

in the micro ring resonator. The refractive index distributed is 1.54 which has been set up to be equivalent to the value of Silicon Oxide, SiO₂.

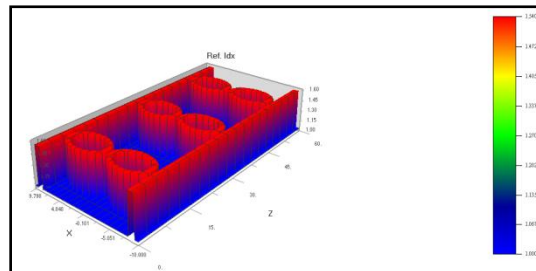


Figure 6: Relative refractive index on the proposed structure

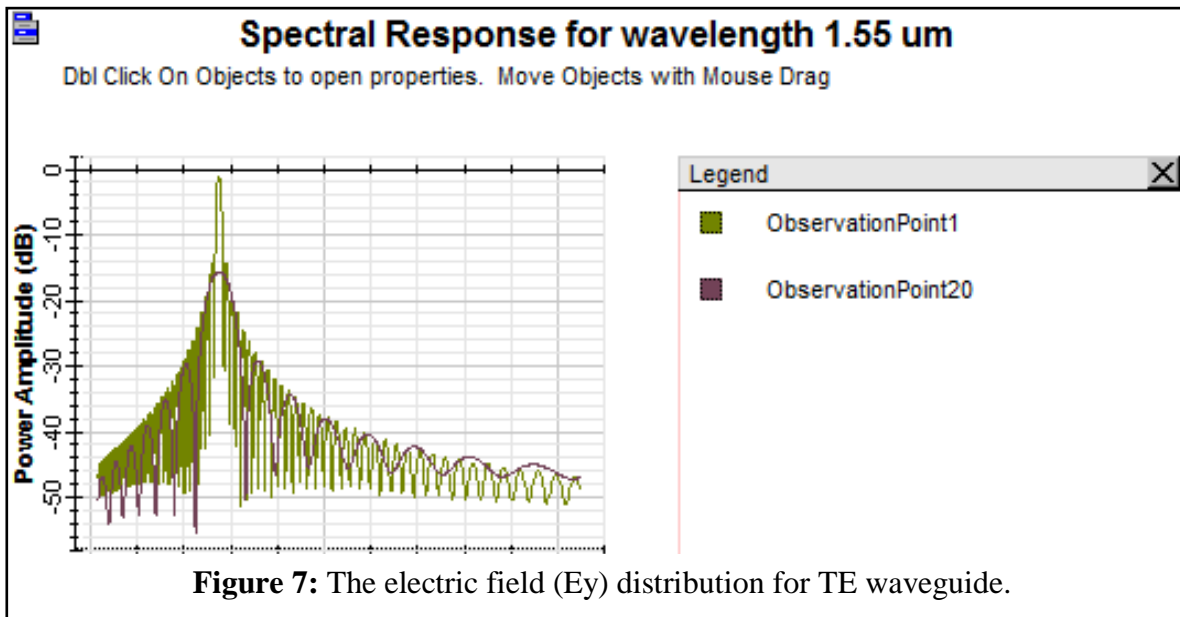


Figure 7: The electric field (Ey) distribution for TE waveguide.

Figure 7 above shows the electric field distribution for the upper linear waveguide when we apply power

through waveguide is decreased for wavelength 1.55 μm .

The power at first observation point is approximately -1.31 dB and decreases to -15.85 dB at the end of the linear waveguide. The power losses when it being transmitted is approximately 14.54 dB.

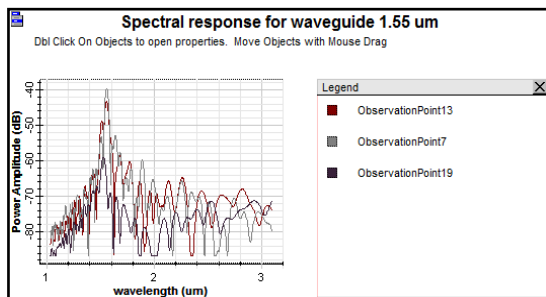


Figure 8: The electric field (E_y) distribution for TE waveguide for lower linear waveguide.

Figure 8 above shows the electric field distribution for the upper linear waveguide when we apply power throughout the configurations. We can clearly observed that the power emit through waveguide is decreased for wavelength 1.55 μm . It shows that some are being transmitted into the ring and lower linear waveguide. Point 7 denotes that the amplitude power manage to be transmitted through the double ring are approximately -39.58 dB.

IV. CONCLUSION

Twisted Double Channel SCISSORS was successfully design for optical filter application. The changes of refractive index in the medium when power propagated throughout the bus waveguide in the micro ring resonator were investigated. A filter characteristics was determined when the power emit through waveguide was decreased for wavelength 1.55 μm .

V. ACKNOWLEDGEMENT

We would like to thank the Institute of Advanced Photonic Science, Faculty of Science, Universiti Teknologi Malaysia (UTM) and University of Riau for generous support in this research.

REFERENCES

- [1] D. G. Rabus, "Integrated Ring Resonator : The Compendium" Springer Series in Optical Sciences, Vol. 127, (2007)
- [2] K. S. Yee, "Numerical solution of initial boundary value problem

- involving Maxwell's equation in isotropic media,*" IEEE Transaction on Antennas and Propagation, vol. AP-14, pp 302-307, 1966.
- [3] A. Taflove and M. E. Brodwin, "*Numerical solution of steady state electromagnetic scattering problems using time dependent Maxwell's equations,*" IEEE Transaction on Microwave Theory and Techniques, pp. 623-630, 1975.
- [4] R. Courant, K. Friedrichs and H. Lewy, "*On the partial difference equations of mathematical physics,*" IBM Journal of Research and Development, 11(2), pp. 215-234, 1967.
- [5] W. Bogaerts, P. Dumon, D. Van Thourhout, D. Taillaert, P. Jaenen, J. Wouters, S. Beckx, V. Wiaux and R. Baets, "Compact wavelength-selective functions in silicon-on-insulator photonics wires," J. Sel. Top. Quantum Electron, vol. 12, no.6, pp. 1394-1401, (2006).
- [6] P. Dumon, W. Bogaerts, V. Wiaux, J. Wouters, S. Becks, J. Van Campenhout, D. Taillaert, B. Luyssaert, P. Bientman, D. Van Thourhout and R. Baets, "Low-loss SOI photonics wires and ring resonators fabricated with deep UV lithography," IEEE Photon, Technology, Lett., vol. 16, no. 5, pp. 1328-1330, 2004.
- [7] Hong Li and Shaowu Zhang. Soliton Transmission in Twin-core fiber. Physics Dept. Hubei Normal University, China (1999)